Dynamic Light Scattering for the Characterization of Polydisperse Fractal Systems: II. Relation between Structure and DLS Results

Uwe Kätzel, Manuel Vorbau, Michael Stintz*, Torsten Gottschalk-Gaudig, Herbert Barthel**

(Received: 5 July 2007; in revised form: 20 November 2007; accepted: 26 November 2007; published online: 12 February 2008)

DOI: 10.1002/ppsc.200700005

Abstract

Dynamic light scattering (DLS) is frequently used to characterize suspensions of pyrogenic silica which consists of polydisperse fractal aggregates of sintered spherical primary particles. As the method primarily measures temporal fluctuations of scattered light caused by the translational and rotational diffusive motion of the aggregates it is an important prerequisite to identify those structural properties that are measurable with DLS and to quantify the method's sensitivity to changes in these properties. In a recent paper [1] we have investigated the structure-hydrodynamics relationship via simulations. Here, the validation of the simulation results by experimental data is presented. Therefore, the structure of different pyrogenic silica grades has been characterized by static light and X-ray scattering and the diffusional properties were obtained by multi-angle DLS measurements. It is shown that the hydrodynamic radii determined with DLS scale well with the mean aggregate radius of gyration but that the influence of rotational diffusion has to be accounted for in the measurements.

Keywords: dynamic light scattering, fractal aggregates, pyrogenic silica, static scattering

1 Introduction

Pyrogenic (or fumed) materials are produced by combustion or other high temperature processes, e.g., technical pyrogenic silica evolves in the hydrolysis of silicon tetrachloride in a hydrogen/oxygen flame:

$$SiCl_4 + 2H_2 + O_2 \rightarrow SiO_2 + 4HCl$$

Flame synthesis that allows for the production of a variety of chemically very pure materials has become very popular in the last years [2–5]. Due to the generation process the particles often show a complex structure. Firstly, in the flame very small protoparticles consisting of only a few SiO_2 molecules are produced that collide and sinter completely to form nearly spherical primary particles of 5–100 nm in size. These primary particles afterwards are still solidifying so that upon collision again an incomplete sintering occurs. Then, aggregates are formed that are 100–500 nm in size. The structure of these aggregates can be best modeled as self-similar fractals [6]. This essentially means that the scale of an aggregate obeys a power law between its volume or mass and its size:

$$m \sim R_g^{D_f} \tag{1}$$

The exponent D_f is called the mass-fractal dimension. It can take values between 1 (for a linear chain) and 3 (a

* Dipl.-Ing. U. Kätzel, Dipl.-Ing. M. Vorbau, PD Dr.-Ing. habil. M. Stintz (corresponding author), Research Group Mechanical Process Engineering, Institute of Process Engineering and Environmental Technology, TU Dresden, D-01062 Dresden (Germany).
E-mail: michael.stintz@tu-dresden.de

** Dr. rer. nat. T. Gottschalk-Gaudig, Dr. rer. nat. H. Barthel, Wacker-Chemie AG, Werk Burghausen, Johannes-Hess-Str. 24, D-84480 Burghausen (Germany).

compact body). The equivalent aggregate radius is the radius of gyration defined as:

$$R_g = \sqrt{\frac{\sum_{i=1}^{N_{prim}} m_i \left|\vec{r}_i - \vec{r}_{cg}\right|^2}{\sum_{i=1}^{N_{prim}} m_i}} \tag{2}$$

where m_i and $\vec{r}_i$ are the mass and the position vector of the i-th primary particle and $\vec{r}_{cg}$ is the position vector of the center of gravity of the cluster. For pyrogenic silica it has been obtained via TEM investigations that the size of the primary particles in a single aggregate does not vary much [7], so Eqs. (1) and (2) can be simplified:

$$N_{prim} = k_f \left(\frac{R_g}{R_{prim}}\right)^{D_f} \tag{3}$$

$$R_g = \sqrt{\frac{1}{N_{prim}} \sum_{i=1}^{N_{prim}} \left|\vec{r}_i - \vec{r}_{cg}\right|^2} \tag{4}$$

The structure and size of pyrogenic aggregates can be tuned by changing the parameters of the flame or the burner [2, 3]. For pyrogenic silica different grades are industrially produced. These are most often distinguished by their specific surface area S_m determined from gas adsorption (BET. i.e., Brunauer-Emmett-Teller surface area). Commercially available silica ranges from 50–400 m^2/g. However, it is not only the size of the primary particles that is altered between the grades but also their distribution. Low specific surface area grades possess a broad distribution of primary particle sizes while high specific surface area grades generally show a narrow distribution. Figure 1 gives two TEM micrographs that visualize the difference.

The structure of fractal aggregates can most easily be characterized by static light scattering (SLS) or small-angle X-ray (SAXS) and neutron scattering (SANS). In liquid applications (where pyrogenic silica is often used as abrasive, thixotropic or thickening agent and as anti-settling agent) the characterization of the disperse state is mostly carried out by dynamic light scattering (DLS). DLS, however, primarily measures fluctuations of scattered light at a certain scattering angle that are caused by diffusive motions of the particles [8–10]. The determined diffusion coefficients can be converted to a hydrodynamic aggregate radius via the Stokes-Einstein equation:

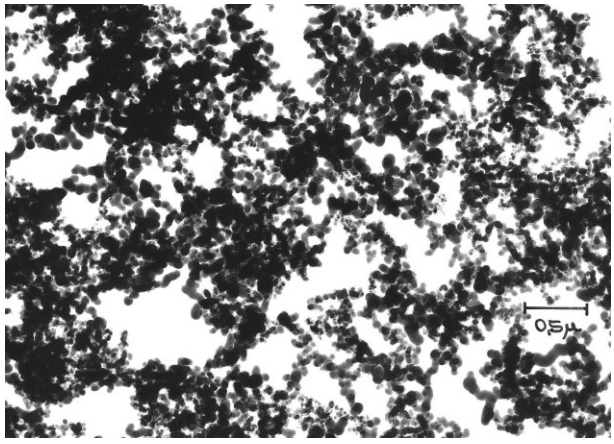

(a)

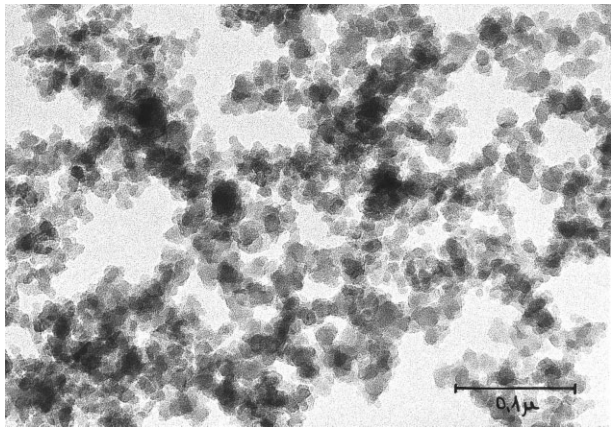

(b)

Fig. 1: Transmission electron micrographs of pyrogenic silica with a) S_m = 50 m^2/g and b) S_m = 300 m^2/g, please note the different scales of the images.

$$D = \frac{k_B T}{6 \pi \eta R_h} \tag{5}$$

where k_B is Boltzmann's constant, T is the temperature, η is the viscosity of the suspension medium and R_h is the radius of a sphere with the same hydrodynamic drag as the particle under consideration. In a recent paper we have investigated the theoretical relationship between the structural properties of fractal aggregates and the hydrodynamic radius determinable with DLS [1]. As the simulations employed there naturally involved some simplifications, comparative measurements have to be conducted to transfer the results to real industrial particle systems.

In this paper we present a comprehensive experimental study on the relation between the structure and hydrodynamics of pyrogenic silica and consequently a comparison to our simulation data. First we will shortly summarize the simulation results that are essential for the

comparison. Section 3 then gives the basics for the structural investigations and the DLS measurements. In section 4 the materials and methods that have been used in the experiments are described. Section 5 is devoted to the measurements of the structural properties of pyrogenic silica while section 6 plays with the DLS experiments. A comparison between experiments and simulation is then given in section 7.

2 Recapitulation of Simulation Results

The most important result of our simulations (see [1] for details) was the relation between the hydrodynamic radius of translation and the radius of gyration for different sizes and fractal dimensions of the considered aggregates. This relation was shown to hold for every fractal-like generation mechanism. However, for pyrogenic silica Schaefer and Hurd [11] proposed a diffusion-limited cluster aggregation (DLCA) [12, 13] of the primary particles as being the most realistic scenario describing the generation process. Such a process yields aggregates with a fractal dimension of 1.86 for very large numbers of primary particles [14, 15] but for small aggregates we have shown that the resulting aggregates show varying fractal dimensions between 1.5 and 1.85 [1]. This range together with the usually observed number of primary particles per aggregate (between 10 and 1000 as obtained from TEM investigations [16]) gives the final result that the hydrodynamic radius of translation $R_{h,t}$ should be somewhat smaller than the radius of gyration with values between $0.7 \ldots 1.0 \cdot R_g$. This ratio should be measurable with static and dynamic scattering techniques.

However, the rotation of aggregates also has an influence on DLS results. Every change of the positions of the scattering centers of the aggregate in the measurement volume leads to fluctuations in the scattered light intensity. Due to the open structure of the fractal aggregates impacts of solvent molecules may cause relatively larger torques compared to compact particles of the same mass. Therefore, rotational diffusion is also reflected in the scattered light so that the *true* hydrodynamic radius of translation can only be determined from measurements at multiple scattering angles [1,9,17,18].

Another important result of our simulations that must be mentioned here is that the hydrodynamic radii also show a fractal scaling that can be described with a power law (cf. Eq. (3)) but that the exponents can be different. Therefore, the concept of hydrodynamic dimensions D_f^h has been introduced with:

$$N_{prim} = k_f^{h,t}\left(\frac{R_{h,t}}{R_{prim}}\right)^{D_f^{h,t}} = k_f^{h,rot}\left(\frac{R_{h,rot}}{R_{prim}}\right)^{D_f^{h,rot}} \quad (6)$$

For DLCA aggregates that should resemble pyrogenic silica the following numerical values have been obtained:

$$N_{prim} = 1.57\left(\frac{R_g}{R_{prim}}\right)^{1.71} = 1.09\left(\frac{R_{h,t}}{R_{prim}}\right)^{1.96} = 1.07\left(\frac{R_{h,rot}}{R_{prim}}\right)^{1.91} \quad (7)$$

This difference between the fractal dimension $D_f = 1.71$ and the hydrodynamic dimensions will be of importance in the comparison with the experimental values.

3 Theoretical

3.1 Static Scattering Techniques

For the structural investigation of matter a collimated beam is incident on the sample. It is scattered by interactions with the particles in the sample, the dispersed particles as well as the solvent molecules. The mean scattered intensity $\bar{I}$ is recorded in dependence of the observation angle θ. The momentum transfer between the incident field and the scattered field is characterized by the vectorial difference of the respective wave vectors $\vec{k}_{inc}$ and $\vec{k}_{sca}$, the scattering vector $\vec{s}$. Its magnitude can be computed from triangular relations under the assumption of elastic scattering (i.e., no frequency change of the scattered wave compared to the incident wave):

$$|\vec{s}| = s = \frac{4\pi n}{\lambda_0}\sin\left(\frac{\theta}{2}\right) \quad (8)$$

where n is the refractive index of the medium and λ_0 is the wavelength of the incident beam in vacuum.

The inverse of the scattering vector has a unit of length and can be understood as being the structure size of matter under investigation. By using SAXS or SANS (s-range: 0.01–1 nm^{-1}) and SLS (s-range: 0.002–0.03 nm^{-1}) several orders of magnitude can be spanned.

If fractal-like particle systems are investigated with static scattering typical patterns as the one given in Figure 2 are obtained. If this pattern is investigated from low to high s-values the same happens as when the magnification of a microscope is increased.

At low s the scattered light intensity is proportional to the volume of the aggregate (assuming Rayleigh-Debye-Gans scattering) [19]. As the volume does not change in the sample a constant value is measured. The constant level is followed by an exponential decay of the scattered intensity. Guinier [20] showed that this can be

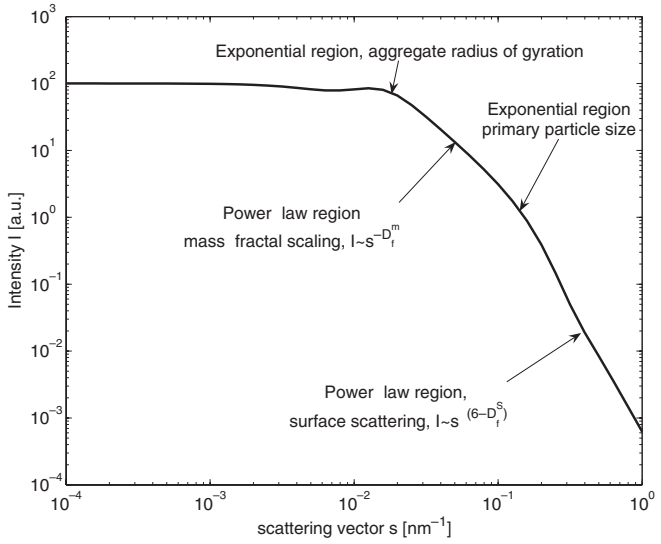

Fig. 2: Model scattering pattern of fractal aggregates with primary particle size of 31.6 nm, aggregate radius of gyration 200 nm, mass and surface fractal dimensions 1.8 and 2.2, respectively. Computed using the unified equation of Beaucage [23,24].

associated with a characteristic size of the structure under investigation. There are two Guinier regimes in Figure 3, the one at lower q can be related to the aggregate radius of gyration while the other one is a measure of the primary particle radius of gyration:

$$I(s) \sim \exp\left(-s^2 \frac{R_g^2}{3}\right) \tag{9}$$

In between this two exponential regimes the decay of the scattered light intensity follows a power-law that describes the mass-fractal scaling inside the aggregate:

$$I(s) \sim s^{-D_f} \tag{10}$$

At even higher q again a power-law behavior is observed. This is the Porod regime [21, 22] where the surface fractal dimension D_f^S of the primary particles may be obtained via:

$$I(s) \sim s^{-(6-D_f^S)} \tag{11}$$

The surface fractal dimension describes the roughness of the surface with values between 2 (perfect sphere) and 3 (very rough surfaces). At larger s the material is then probed at atomic levels (crystallinity and crystal structures, not shown in Figure 2).
In practice, the different exponential and power-law regions cannot be easily distinguished. Therefore, Beaucage developed a unified equation that is able to fit a whole measured scattering pattern to give the fractal dimensions and the size parameters [23, 24]. By using further analyses also the specific surface area can be determined [25].

3.2 Dynamic Light Scattering

Particles in liquids are in permanent motion due to non-compensated impacts of the solvent molecules. If a light beam impinges on such particles the observed scattered light intensity shows temporal variations caused by an optical Doppler effect. Most DLS instruments compute the second-order intensity auto-correlation function (ACF):

$$g_2(\tau) = \frac{\langle I(t)\, I(t+\tau)\rangle}{\langle I(t)\rangle^2} \tag{12}$$

that is related to the first-order electric field correlation function (FCF) via the Siegert-relation [26]:

$$g_2(\tau) = 1 + b\, g_1(\tau)^2 \tag{13}$$

Here, τ is the lag time of the correlator and b is the coherence factor of the measurement instrument which is dependent on the detector area, the optical alignment and the scattering properties of the system. In diluted suspensions, values of 0.9–1 can be achieved.
The solution of Fick's second law in the domain of the scattering vector reveals that the FCF is a simple exponential for monodisperse particles of size x and diffusion coefficient D:

$$g_1(\tau) = \exp\left(-Ds^2\tau\right) \tag{14}$$

For polydisperse systems each particle contributes weighted by its scattering efficiency and the FCF then reads:

$$g_1(\tau) = \int_0^\infty q_{\text{int}}(D) \exp(-Ds^2\tau)\; dD \tag{15}$$

The determination of $q_{int}(D)$ from Eq. (15) poses some mathematical difficulties. Eq. (15) is a Fredholm integral equation of the first kind, which can in principle be solved by an inversion after discretization. However, the measurement error causes that usually an infinite number of equally probable solutions may be found. Thus, data analysis is either carried with methods that only determine some mean values and moments of $q_{int}(D)$ and require no a priori information or with Laplace inversion schemes that incorporate several boundary conditions to deal with the ill-conditioned nature of Eq. (15) [27–29]. For our purposes only the so-called second cumulants analysis introduced by Koppel [30] has been

used. The cumulants generating function is just the natural logarithm of the FCF:

$$K(-\tau, s) = \ln|g_1(\tau, s)| \tag{16}$$

The cumulants $K_i(s)$ are defined as the coefficients of an expansion of $K(-\tau,s)$ in a MacLaurin series:

$$K(-\tau, s) = \sum_{i=1}^{\infty} K_i(s) \frac{(-\tau)^i}{i} \tag{17}$$

Usually, only the two first cumulants can be determined with low uncertainty from experimental data [30]:

$$K_1 = D_{eff} = \int_0^{\infty} D\, q(D)\, dD \tag{18}$$

$$K_2 = \int_0^{\infty} (D - D_{eff})^2\, q(D)\, dD \tag{19}$$

The first cumulant describes an effective mean diffusion coefficient while the second describes the relative width of the distribution if normalized by $(K_1)^2$. The normalized variable is usually referred to as the polydispersity index *PDI*:

$$PDI = \frac{K_2}{K_1^2} \tag{20}$$

This method is fast, robust and easy to use and is therefore even incorporated in the International Standard ISO 13321 [10].

4 Materials and Methods

In these investigations different pyrogenic silica grades supplied by Wacker-Chemie AG, Burghausen have been used. Table 1 gives an overview of the employed samples and their properties.

Table 1: Employed pyrogenic silica samples and their relevant physical properties.

Silica Grade HDK®	Specific Surface Area S_m (BET) [m^2/g], mean value of specification	Sauter Diameter x_{ST} [nm]
D05	50	54.6
C10P	100	27.2
S13	125	21.8
V15	150	18.2
N20	200	13.6
T30	300	9.0
T40	400	6.8

The Sauter diameter x_{ST} has been computed with:

$$x_{ST} = \frac{6}{S_m\, \rho_s} \tag{21}$$

assuming a solids density ρ_s of 2200 kg/m^3. As the original product is a dry powder an extensive dispersion procedure is necessary to obtain a reproducible state of dispersion. Imperfect dispersion results in the measurement of smaller diffusion coefficients by DLS and has, therefore, to be avoided. Pyrogenic silica was firstly added up to 5 wt.% to a mother solution of 0.001 M potassium nitrate while stirring the liquid. After a 30 min stirring, the suspension was firstly dispersed with a rotor-stator disperser for 10 min at 7000 min^{-1} (UltraTurrax T50, IKA, Germany). Then, the pH of the suspension was adjusted to a value of 9 with KOH to stabilize the silica aggregates and prevent agglomeration. Subsequently, dispersion was finished using an ultrasonic disintegrator (VibraCell VCX 600, 600 W, Sonics and Materials Inc., USA). Sonification lasted for 2 minutes twice. To avoid a strong heating, the probe was used in pulse mode (2 s on / 2 s off). The progress of dispersion was monitored using laser diffraction (HELOS 12 KA/LA, Sympatec GmbH, Germany) after each step. Between the process steps the suspension was cooled. Finally, the pH was again controlled and adjusted. Then, for the SAXS measurements 0.1 wt.% samples were prepared by dilution with the mother solution. For SLS and DLS, a single droplet of the 5 wt.% solution was added to 100 ml of deionized water. To further remove dust contributions the suspensions were filtered through a 20 µm paper filter under clean room conditions. The sample flasks were then sealed and the samples characterized.

SAXS measurements were conducted at the Institute of Mechanical Process Engineering and Mechanics of the University of Karlsruhe. The experimental set-up was a modified Kratky camera with a block collimation system as described by Dingenouts [31]. The measurable s-range was 0.04 nm^{-1} – 1 nm^{-1}. Data analysis involved background correction, desmearing and the structural analysis using the Irena 2 package (Argonne National Laboratory, USA) for Igor Pro (WaveMetrics Inc., USA).

For the SLS measurements we employed a modified FICA 50 (Applied Research Laboratories GmbH, Germany) equipped with a He-Ne gas laser (λ_0 = 632 nm). The angular range of the instrument was 15°–145°. Samples were contained in a temperature-controlled index-matching vat. No

background signal and no refractive index increment was measured since this is not necessary for the structural analysis.

Multi-angle DLS measurements have been performed on an ALV/DLS/SLS-5000 laser light scattering spectrometer (ALV Laservertriebsgesellschaft mbH, Germany) with an ALV-5000/EPP multiple tau correlator and a ALV/CGS-8F S/N 025 goniometer system that provides an angular range of 10°–150°. A He-Ne laser that could be mitigated by a compensated optical attenuator, was used as light source. Laser power stabilization lasted for at least 1 h before a measurement. The cylindrical sample cell was again placed in an index-matching vat with an accuracy of ± 5 μm. Before a measurement run was started temperature of vat and sample were equilibrated for 15 min. For an additional DLS measurement point in the backscattering regime at 173° we used a Malvern HPPS DLS instrument also equipped with a He-Ne gas laser. For each measured scattering angle the data acquisition time was changed according to Eqs. (8) and (14):

$$\frac{t^1_{meas}}{t^2_{meas}} = \frac{\sin\left(\frac{\theta_2}{2}\right)}{\sin\left(\frac{\theta_1}{2}\right)} \tag{22}$$

to probe the same dynamic range and yield the same statistics for each data point of the measured ACF. As a starting time 90 s duration for $\theta = 173°$ was chosen. Data acquisition and analysis was carried out with the ALV Correlator Software V.3.0 for both DLS instruments. For each sample 9 single runs were recorded. Afterwards, a unique ACF was obtained by a randomization procedure where for each lag time an autocorrelation value was chosen randomly from the single runs. This method stabilizes the subsequent data analysis since covariant measurement errors are minimized [32].

5 Structural Properties

The measured SAXS intensity profiles of the pyrogenic silica grades are given in Figure 3. In Figure 3(a) a single scattering profile has been given and the relevant regions designated. Obviously, the determination of the surface fractal dimension and the primary particle size is hampered by the larger uncertainty of the data in this region. From Figure 3(b) it can additionally be concluded that the mass-fractal dimension D_f for low specific surface area grades is influenced by the polydispersity of the samples affecting the linearity in the log-log plot. This difficulty also holds for the aggregate radius of gyration.

Table 2 gives the results of the structural analysis obtained from the unified equation [23,24]. Additionally,

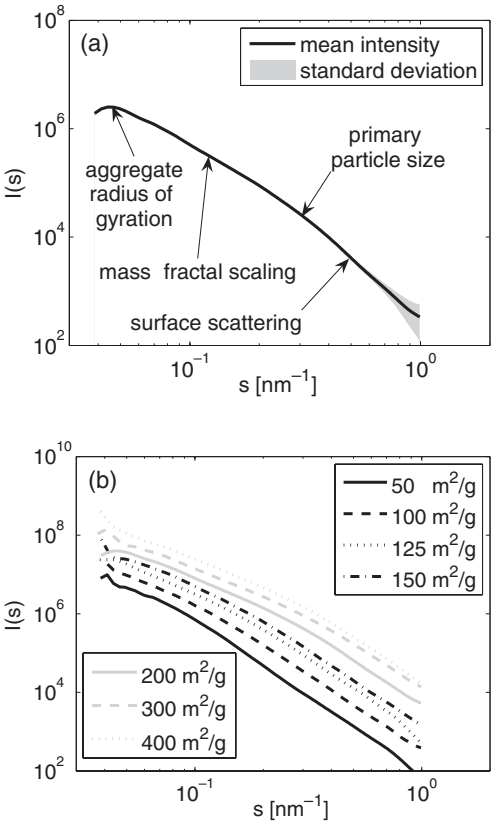

Fig. 3: Measured X-ray scattered intensity profiles for 0.1 wt.% samples of pyrogenic silica in 0.001 M KNO_3 solution at pH 9: (a) Mean intensity and data scatter for a sample with 200 m^2/g specific-surface area, (b) Comparison of different pyrogenic silica grades marked in the diagram. Curves have been shifted on the y-axis for better visual discrimination.

Table 2: Structural properties of pyrogenic silica samples determined from SAXS. The fractal dimension could not be determined for all grades.

S_m (BET) [m^2/g]	S_m (SAXS) [m^2/g]	R_g [nm]	D_f
50	95.1	37.25	–
100	145.4	> 80	2.46
125	158.1	48.92	2.51
150	177.4	30.85	–
200	271.4	31.06	2.48
300	361.7	29.29	2.36
400	297.9	67.25	2.33

the specific surface area has been computed to enable a comparison with the gas adsorption values (BET).

The data do not correspond to the expectations at first sight. The most controversial feature is the large difference in the measured mass-fractal dimension and the value that is expected from the proposed generation mechanism of Schaefer and Hurd [11] (DLCA; $D_f \sim 1.5$–1.85). The deviations here are not only due to

the deformation of the profiles caused by sample polydispersity. There must be other reasons for this behavior.

A second observation which can be made is that the radius of gyration in Table 2 does not correspond to the aggregate size that can be observed with TEM [16]. On the other hand the data can be compared to newly derived SANS results of Bugnicourt et al. [33] who used the same silica grades as in this work. They also obtained fractal dimensions in the range of 2.23–2.61 and radii of gyration between 25–32 nm. However, for one sample they also obtained another radius at low s (~ 210 nm for a 200 m^2/g sample) that was interpreted as an interparticle distance. This order of magnitude is, however, the expected range from TEM analysis. Regarding this expectation it is assumable that the accessible s-range in the SAXS measurements is not sufficient to characterize the whole scattering pattern of pyrogenic silica. This hypothesis is additionally supported by the specific surface area values in Table 2. The computed values are always higher than the gas adsorption measurements (c.f. Table 1). This result should be obtained if large primary particles and aggregates were excluded in the SAXS scattering pattern. The sample with 400 m^2/g specific surface area is the only exception in Table 2 since the primary particles show an intrinsic porosity that is measurable with gas adsorption but invisible for SAXS.

SLS probes smaller s-values than SAXS and may, therefore, serve as a further substantiation of the above made hypothesis. Figure 4 shows the log-log plot of the scattered light intensity over scattering vector.

There are three regimes that can be distinguished among the grades. For high specific surface area values at low s a plateau value is observed that suggests a transition to volume scattering. A Guinier regime related to a radius of gyration can be observed for all grades. However, the exponential decrease is shifted to higher s-values when the specific surface area of the samples is increased. Finally, at large s power-law behavior can be observed corresponding to fractal scaling. The determined fractal dimensions and radii of gyration are summarized in Table 3.

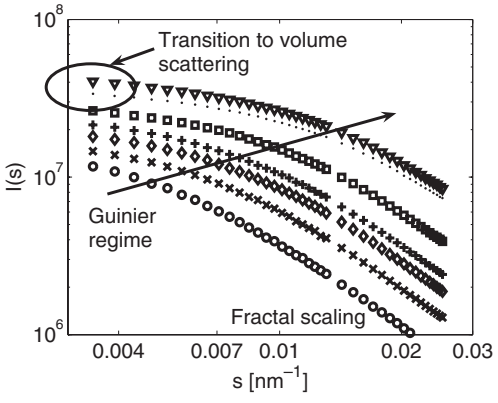

Fig. 4: Measured scattered light intensity profiles for diluted pyrogenic silica suspensions in 0.001 M KNO_3 solution at pH 9. Samples with 50 m^2/g (open circles), 100 m^2/g (crosses), 125 m^2/g (open diamonds), 150 m^2/g (pluses), 200 m^2/g (open squares), 300 m^2/g (dots) and 400 m^2/g (open triangles) specific-surface area. Curves have been shifted on the y-axis for better visual discrimination.

Table 3: Structural properties of pyrogenic silica samples determined from SLS. The uncertainty in fractal dimension rises with increasing specific-surface area.

S_m (BET) [m^2/g]	R_g [nm]	D_f
50	202	1.77
100	187	1.78
125	167	1.76
150	163	1.77
200	140	1.72
300	116	1.54
400	117	1.58

The fractal dimension determined from the slope of the decrease in the log-log plot gives reliable results only for low surface area grades (up to S_m = 150 m^2/g) since more than 15 data points are included in the fit. Uncertainties occur for high specific surface area grades since only 4 or 5 points can be used to determine the fractal dimension that is still influenced by the Guinier regime.

It is, however, striking that both values, D_f and R_g differ remarkably from the SAXS values. The radii of gyration are much larger which is obviously due to the different s-ranges of the two methods. Additionally, there is a clear decrease of the radius of gyration with increasing surface area which was not obtained with SAXS and SANS [33]. As with SLS for some grades the volume scattering plateau is reached, it is likely that the radii of gyration determined here are the *true* aggregate radii.

Contrary, the fractal dimensions are lower for all grades and are even nearly constant for samples with low specific surface area. The values of 1.55–1.78 also rather correspond to the theoretically expected values for a DLCA generation mechanism. However, the SAXS results may not just be dismissed. Clarification can only be anticipated from the dynamic scattering results since the hydrodynamic radii should scale with the radius of gyration of the aggregates as obtained in our simulations [1].

6 Diffusion Measurements

Figure 5 shows the primary measurement result, the autocorrelation functions, for a sample with S_m = 150 m^2/g specific surface area. It is readily available from the figure that the mean decay is shifted towards larger lag times with a reduction of the scattering angle. Thus, the adjustment of the duration of a single measurement run with Eq. (22) is verified.

As a first analysis step the mean diffusion coefficients for each scattering angle have been computed from a second cumulants analysis of the randomized ACF's. Additional to the standard algorithm outlined in section 3.2 we used an additional baseline correction via a low-pass filter of the frequency spectrum obtained from a fast-Fourier transformation of the gradient of the ACF. We then achieve an ACF that decays to zero within the main decay. This procedure accounts for single large agglomerates or dust in the samples and is extremely useful especially for low scattering angles. The obtained mean diffusion coefficients are shown in Figure 6(a) for low specific surface area grades and in Figure 6(b) for high specific-surface area grades.

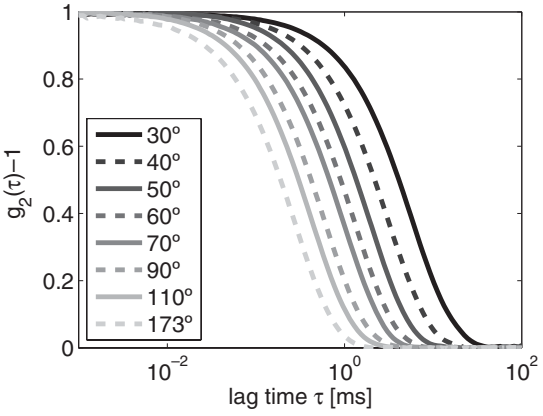

Fig. 5: Autocorrelation functions for a diluted pyrogenic silica suspension (S_m = 150 m^2/g) at different scattering angles.

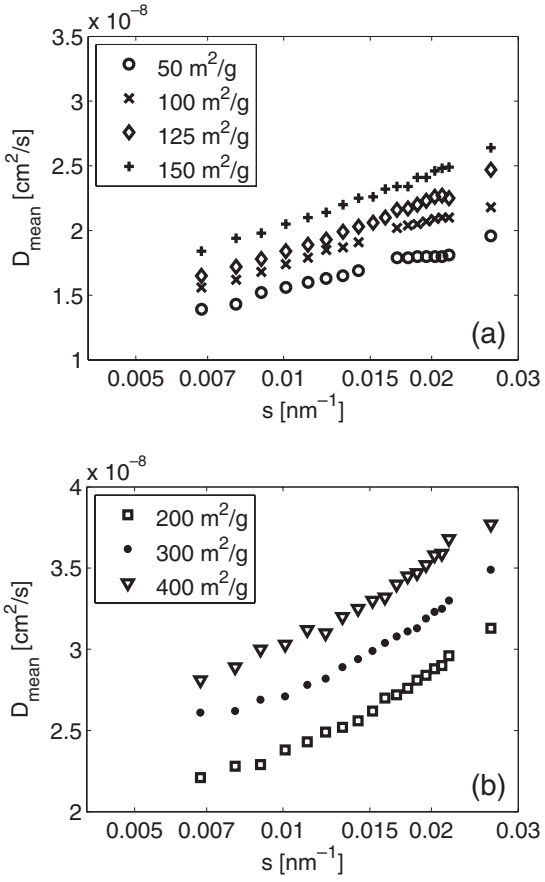

Fig. 6: Mean diffusion coefficients determined from a second cumulants analysis. The influence of rotational diffusion can be recognized from the scattering vector dependence. Note the different scales of the y-axes in the subfigures.

There is a strong variation of the mean diffusion coefficients when the scattering angle is changed. As predicted in our simulations we have to consider the influence of aggregate rotational diffusion here [1]. In view of the evolution of the scattering angle dependence an interesting feature can be observed. For the grades with 300 m^2/g and 400 m^2/g specific-surface area the mean diffusion coefficient seems to approach a plateau value at low s while for the other grades this behavior is not observed. Additionally, the curves resemble the theoretically obtained trend of Lindsay et al. [17] for DLCA aggregates. They obtained an overestimate of the mean diffusion coefficient if $sR_g > 1$ that grows to a plateau of about $1.55 - 1.65 \cdot D(s \to 0)$ for $sR_g > 5$ as obtained in our simulations. Therefore, the following empirical equation approximating this behavior has been used to determine the aggregate translational diffusion coefficient:

$$\frac{\bar{D}}{10^{-8}\,\frac{cm^2}{s}} = C_1 + \frac{C_2}{1 + \left(\frac{\log_{10}(s \cdot m)}{C_3}\right)^{C_4}} \tag{23}$$

An extrapolation to $s \to 0$ gives the desired value. From it, the hydrodynamic radius of translation can be computed using the Stokes-Einstein relation (Eq. (5)). The results are displayed in Table 4.

It can be deduced that the hydrodynamic radii are always smaller but comparable to the radius of gyration determined with SLS (c.f. Table 3). This result substantiates the above made hypothesis that the size measured with static light scattering corresponds to the *true* aggre-

Table 4: Hydrodynamic radii of translation determined from extrapolating multi-angle DLS cumulants analysis results to vanishing scattering vector with Eq. (23).

S_m (BET) [m^2/g]	$R_{h,t}$ [nm]
50	199.4
100	170.9
125	157.2
150	140.1
200	114.8
300	97.0
400	92.1

gate radius. It has to be noted that the plateau value D_∞/D_0 can only be extrapolated with small uncertainty for the lowest specific-surface area grade. The results 1.55 (50 m^2/g) and 1.66 (100 m^2/g) suggest a relation to our simulation results and to the results of Lindsay et al. [17], however, a clear prove could only be received from measurements at even larger scattering vectors (which is not achievable using dynamic light scattering at 632.8 nm wavelength).

7 Comparison

If we directly compare the ratio $R_{h,t}/R_g$ (see Table 5) we obtain values between 0.787 and 0.987. This range has been predicted in the simulations (c.f. section 2). This supports the assumption that the best description of the generation process of pyrogenic silica is a DLCA mechanism.

Now, the ratios can additionally be employed to estimate the mean number of primary particles per aggregate from our simulations (c.f. Figure 7 in [1]). Therefore, we assume an equal fractal dimension of 1.8 for all samples accounting for the SLS results and the simulations. The obtained numbers are between 90 and 1000 which is in good agreement to the observations made by TEM imaging [16]. The obtained trend is naturally clear

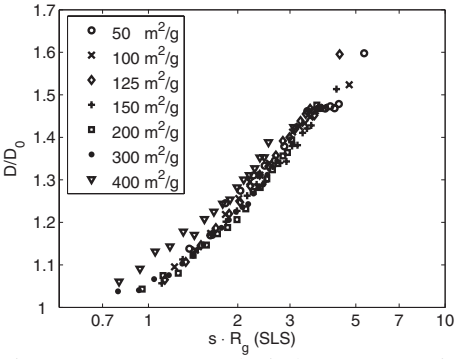

Fig. 7: Master-curve of the influence of rotational diffusion on the mean diffusion coefficient D measured with DLS. The values are scaled with the corresponding translational diffusion coefficient obtained at $s \to 0$. The scattering vector is scaled with the radius of gyration R_g from SLS. Plot as in the simulations of Lindsay et al. [17].

as, e.g., low specific-surface area grades possess larger primary particles so they must show lower numbers of primary particles. If we now use Eq. (7) which was obtained in the simulations for DLCA aggregates to compute the mean primary particle radius R_{prim} of the samples from the N_{prim} and $R_{h,t}$ we obtain values that are in a fairly good agreement to the radii determined from gas adsorption (c.f. Table 1). This is another indication of the reliability of our simulations and the good comparability between SLS and DLS.

If we finally plot the mean diffusion coefficients normalized with translational diffusion coefficient D_0 ($s = 0$) against the scaled structural axis $s \cdot R_g$ (SLS) in Figure 7 an interesting observation can be made. The data points form a master-curve for all silica grades except for the one with S_m = 400 m^2/g specific-surface area. As mentioned earlier deviations in this grade may be due to an intrinsic porosity of the primary particles caused by the production process.

This master-curve strongly resembles the simulation results of Lindsay et al. [17] for DLCA clusters. Though, the upper plateau predicted with 1.7 by Lindsay et al.,

Table 5: Comparison of structural and hydrodynamic properties of pyrogenic silica with simulation results.

S_m (BET) [m^2/g]	$R_{h,t}/R_g$	N_{prim} estim. from Figure 1 using $D_f = 1.8$	R_{prim} (Eq. (7)) with $R_{h,t}$ and N_{prim} [nm]
50	0.987	90	21.0
100	0.914	220	11.4
125	0.941	180	11.6
150	0.856	300	8.0
200	0.820	550	4.8
300	0.836	450	4.5
400	0.787	1000	2.8

1.55–1.65 by our simulations [1] and 1.45 by Lattuada et al. [18] cannot be determined exactly in our measurements. However, no measured data point exceeds the upper limit so our simulation results are again validated.
The interpretation of the SAXS results is still an open question. A hypothetical explanation may be found in the generation process. In the hot zone of the flame, where the primary particles are produced, there is a large number concentration and the particles are still solidifying. Thus, the aggregation is mostly driven by primary particle – primary particle collisions with a large sintering factor. Small but strongly sintered aggregates are generated. Further down the flame, the temperature drops as well as the primary particle concentration. Now, cluster-cluster aggregation predominates and sintering is reduced. Now, the final aggregates evolve but only with a loose sintered contact. This finally means that an aggregate measured with DLS and SLS may consist of smaller and strongly-sintered sub-aggregates which could explain the measured radii of gyration and fractal dimensions within SAXS. Surely, this assumption has to be substantiated, so future investigations should focus on closing the gap in *s*-range in static scattering (e.g., using Ultra-Small Angle X-ray Scattering) and dynamic scattering. This would enable a unified analysis of the complete scattering pattern as well as an exact determination of the upper and lower plateau values of the mean diffusion coefficient.

8 Summary

The interpretation of dynamic light scattering data for pyrogenic silica is of great relevance for technical applications but is hampered by the fractal structure of the aggregates. After having investigated the relationship between structure descriptors (radius of gyration, mass-fractal dimension) and the hydrodynamic behavior in an earlier paper [1] we have now validated our simulation results with experimental data at commercially available pyrogenic silica powders. The radius of gyration and the fractal dimension were determined from the scattered intensity patterns of static light and X-ray scattering and the hydrodynamic aggregate radii were obtained from multi-angle DLS (extrapolated to $s \rightarrow 0$). As obtained in our simulations for a diffusion-limited cluster aggregation the measured radii of SLS and DLS scale with each other (ratio $R_{h,t}/R_g$ between 0.787 and 0.987). The fractal dimension determined with SLS also resembles a DLCA generation mechanism. However, the structural properties determined with SAXS differ remarkably from the SLS results. Since both methods measure at different ranges of the scattering vector this suggests that different details of the aggregate structure are observed. For SAXS, the strong sintering of primary particles at the beginning of the aggregation process has been hypothesized to explain the large fractal dimensions measured at sub-structures of the aggregates.
The results of DLS show a strong angular dependence caused by influences of rotational diffusion. On a normalized plot all non-porous silica grades form a master-curve. Such behavior had been predicted from the simulations. This shows that the polydispersity of the primary particles in the silica grades does not influence the comparability of structural and diffusional analysis of pyrogenic silica as both mean values show a good correlation.
To directly obtain information on rotational diffusion of fractal aggregates depolarized dynamic light scattering is a valuable tool that will be examined in further investigations. Hopefully then structural information from the hydrodynamic radius of translation and rotation, respectively, can be merged to get an even more comprehensive insight into the structure and behaviour of polydisperse fractal systems.

9 Acknowledgements

The authors wish to thank Wacker-Chemie AG, Burghausen, Germany, for the financial support of this study.

10 Nomenclature

Symbols

b	–	coherence factor
C	–	constant
D	$m^2 \cdot s^{-1}$	diffusion coefficient
D_f	–	mass-fractal dimension
g_1	–	normalized electric-field correlation function
g_2	–	second-order intensity correlation function
I	a.u.	intensity
K	a.u.	cumulant of a distribution
k_B	$J \cdot K^{-1}$	Boltzmann's constant
k_f	–	fractal prefactor
m	kg	mass
N	–	number
n	–	medium refractive index
PDI	–	polydispersity index
q	$s \cdot m^{-2}$	probability density
r	m	distance or position
R	m	radius
s	m^{-1}	magnitude of the scattering vector

S_m	$m^2 \cdot kg^{-1}$	specific-surface area
T	K	temperature
t	s	time
x	m	particle size
η	Pa·s	viscosity
θ	–	observation angle
λ	m	wavelength
τ	s	lag time

Abbreviations

a.u.	arbitrary units
ACF	Auto-Correlation Function
BET	Brunauer-Emmett-Teller model for gas adsorption measurement
DLCA	Diffusion-Limited Cluster Aggregation
DLS	Dynamic Light Scattering
FCF	Field-Correlation Function
SANS	Small-Angle Neutron Scattering
SAXS	Small-Angle X-Ray Scattering
SLS	Static Light Scattering
TEM	Transmission Electron Microscopy

11 References

[1] U. Kätzel, R. Bedrich, M. Stintz, R. Ketzmerick, T. Gottschalk-Gaudig, H. Barthel, Dynamic Light Scattering for the Characterization of Polydisperse Fractal Systems: I. Simulation of the Diffusional Behavior. *Part. Part. Syst. Charact.* **2008**, *25*, 9–18.

[2] S. E. Pratsinis, Gas Phase Synthesis of Nanoparticles, in *Frontiers in Particle Science and Technology* (Eds.: D. T. Goddard, S. Lawson, R. A. Williams), Alphagraphics, Leeds, **2002**.

[3] R. Mueller, H. K. Kammler, S. E. Pratsinis, A. Vital, G. Beaucage, P. Burtscher, Non-Agglomerated Dry Silica Nanoparticles. *Powder Technol.* **2004**, *140*, 40–48.

[4] H. Schulz, W. J. Stark, M. Maciejewski, S. E. Pratsinis, A. Baiker, Flame-made Nanocrystalline Ceria/Zirconia Doped with Alumina or Silica: Structural Properties and Enhanced Oxygen Exchange Capacity. *J. Mater. Chem.* **2003**, *13*, 2979–2984.

[5] R. Strobel, A. Baiker, S. E. Pratsinis, Aerosol Flame Synthesis of Catalysts. *Adv. Powder Technol.* **2006**, *17*, 457–480.

[6] B. B. Mandelbrot, *The Fractal Geometry of Nature.* W.H. Freeman, New York, **1982**.

[7] H. Barthel, T. Gottschalk-Gaudig, personal communication.

[8] R. Finsy, Particle Sizing by Quasi-Elastic Light Scattering. *Adv. Colloid Interface Sci.* **1994**, *52*, 79–143.

[9] R. Xu, *Particle Characterization: Light Scattering Methods.* Kluwer Academic Publishers, London, **2000**.

[10] International Standard ISO 13321: *Particle Size Analysis: Photon Correlation Spectroscopy.* Beuth-Verlag, Berlin, **1996**.

[11] D. W. Schaefer, A. J. Hurd, Growth and Structure of Combustion Aerosols. *Aerosol. Sci. Technol.* **1990**, *12*, 876–890.

[12] P. Meakin, Formation of Fractal Clusters and Networks by Irreversible Diffusion-Limited Aggregation. *Phys. Rev. Lett.* **1983**, *51*, 1119–1122.

[13] M. Kolb, L. Botet, R. Jullien, Scaling of Kinetically Growing Clusters. *Phys. Rev. Lett.* **1983**, *51*, 1123–1126.

[14] M. Y. Lin, H. M. Lindsay, D. A. Weitz, R. Klein, R. C. Ball, P. Meakin, Universality in colloid aggregation. *Nature* **1989**, *339*, 360–362.

[15] M. Y. Lin, H. M. Lindsay, D. A. Weitz, R. Klein, R. C. Ball, P. Meakin, Universal diffusion-limited colloid aggregation. *J. Phys.: Condens. Matter* **1990**, *2*, 3093–3113.

[16] H. Barthel, T. Gottschalk-Gaudig, personal communication.

[17] H. M. Lindsay, R. Klein, D. A. Weitz, M. Y. Lin, P. Meakin, Effect of Rotational Diffusion on Quasielastic Light Scattering. *Phys. Rev. A* **1988**, *38*, 2614–2626.

[18] M. Lattuada, H. Wu, M. Morbidelli, Rotational Diffusivity of Fractal Clusters. *Langmuir* **2004**, *20*, 5630–5636.

[19] M. Kerker, *The Scattering of Light and other Electromagnetic Radiation.* Academic Press, New York, **1969**.

[20] A. Guinier, J. Fournet, *Small-Angle Scattering of X-Rays.* John Wiley & Sons, New York, **1955**.

[21] G. Porod, Die Röntgenkleinwinkelstreuung von dichtgepackten kolloiden Systemen. 1. Teil. *Kolloid-Z.* **1951**, *124*, 83–114.

[22] G. Porod, Die Röntgenkleinwinkelstreuung von dichtgepackten kolloiden Systemen. 2. Teil. *Kolloid-Z.* **1952**, *125*, 51–57, 109–122.

[23] G. Beaucage, Approximations Leading to a Unified Exponential/Power-Law Approach to Small-Angle Scattering. *J. Appl. Cryst.* **1995**, *28*, 717–728.

[24] G. Beaucage, Small-Angle Scattering from Polymeric Mass Fractals of Arbitrary Mass Fractal Dimension. *J. Appl. Cryst.* **1996**, *29*, 134–146.

[25] J. Hyeon-Lee, G. Beaucage, S. E. Pratsinis, S. Vemury, Fractal Analysis of Flame-Synthesized Nanostructured Silica and Titania Powders Using Small-Angle X-Ray Scattering. *Langmuir* **1998**, *14*, 5751–5756.

[26] A. J. F. Siegert, On the Fluctuations in Signals Returned by Many Independently Moving Scatterers. *MIT Rad. Lab. Rep.* **1943**, *465*.

[27] S. L. Nyeo, B. Chu, Maximum-Entropy Analysis of Photon Correlation Spectroscopy Data. *Macromolecules* **1989**, *22*, 3998–4009.

[28] S. W. Provencher, A Constrained Regularization Method for Inverting Data Represented by Linear Algebraic or Integral Equations. *Comp. Phys. Comm.* **1982**, *27*, 213–227.

[29] J. Honerkamp, D. Maier, J. Weese, A Nonlinear Regularization Method for the Analysis of Photon Correlation Spectroscopy Data. *J. Chem. Phys.* **1993**, *98*, 865–872.

[30] D. E. Koppel, Analysis of Macromolecular Polydispersity in Intensity Correlation Spectroscopy: The Method of Cumulants. *J. Chem. Phys.* **1972**, *57*, 4814–4820.

[31] N. Dingenouts, *Röntgenkleinwinkelstreuung als Methodik der Strukturanalyse teilgeordneter kolloidaler Systeme.* PhD Thesis, University of Karlsruhe, **1999**.

[32] R. Peters, Noise on Photon Correlation Functions and its Effect on Data Reduction Algorithms, in *Dynamic Light Scattering: The method and some applications* (Ed.: W. Brown), Clarendon Press, Oxford, **1993**, pp. 149–176.

[33] E. Bugnicourt, J. Galy, J.F. Gérard, F. Boué, H. Barthel, Structural Investigations of Pyrogenic Silica – Epoxy Composites by Small-Angle Neutron Scattering and Transmission Electron Microscopy, **2006**, submitted for publication.

